

SIMULATIONS OF DUST IN INTERACTING GALAXIES I: DUST ATTENUATION

PATRIK JONSSON

Department of Astronomy and Astrophysics, University of California, Santa Cruz, CA 95064

T. J. COX¹ AND JOEL R. PRIMACK

Department of Physics, University of California, Santa Cruz, CA 95064

AND

RACHEL S. SOMERVILLE

Space Telescope Science Institute, 3700 San Martin Drive, Baltimore MD 21218

Submitted to ApJ.

ABSTRACT

A new Monte-Carlo radiative-transfer code, *Sunrise*, is used in conjunction with hydrodynamic simulations of major galaxy mergers to calculate the effects of dust in such systems. The simulations are in good agreement with observations of dust absorption in starburst galaxies, and the dust has a profound effect on their appearance. The dust attenuation increases with luminosity such that at peak luminosities $\sim 90\%$ of the bolometric luminosity is absorbed by dust. In general, the detailed appearance of the merging event depends on the stage of the merger and the geometry of the encounter. The fraction of bolometric energy absorbed by the dust, however, is a robust quantity that can be predicted from the intrinsic properties bolometric luminosity, baryonic mass, star-formation rate, and metallicity of the system. This paper presents fitting formulae, valid over a wide range of masses and metallicities, from which the absorbed fraction of luminosity (and consequently also the infrared dust luminosity) can be predicted. The attenuation of the luminosity at specific wavelengths can also be predicted, albeit with a larger scatter due to the variation with viewing angle. These formulae for dust attenuation appear to be valid for both isolated and interacting galaxies, are consistent with earlier studies, and would be suitable for inclusion in theoretical models, e.g. semi-analytic models of galaxy formation.

Subject headings: dust — radiative transfer — galaxies: interactions — galaxies: starburst — methods: numerical

1. INTRODUCTION

Galaxy mergers produce some of the most spectacular events in the universe. Locally, they are responsible for the most luminous objects, Ultraluminous Infrared Galaxies (ULIRGs, Sanders & Mirabel 1996). At higher redshifts they may be responsible for the sources seen in the submillimeter (Smail et al. 1997), and they may even be a dominant mode of star formation in the early universe (Somerville et al. 2001; Elbaz & Cesarsky 2003, but see Wolf et al. 2004). Because the most luminous objects are also generally the most dust-obscured, it was not until the launch of IRAS that the existence of ULIRGs was discovered. What in the optical appeared to be fairly unimpressive, albeit peculiar, galaxies turned out to be the brightest infrared sources in the local universe. It is now clear that starbursts and dust generally go hand-in-hand. The large amounts of gas necessary to fuel a major starburst bring with them large column densities of dust, obscuring the starburst and reradiating the energy in the far infrared. In addition, rapid star formation quickly enriches the region with metals, increasing the amount of dust further. Including the effects of dust is thus crucial when studying these systems.

Theoretical studies of dust in galaxies have generally not leveraged the power of hydrodynamic simulations but rather used fairly simple geometries. Gordon et al. (1997), using a Monte-Carlo radiative-transfer model, concluded that Small-Magellanic-Cloud-type (as opposed to Milky-Way-type) dust was necessary to fit observations of starburst galaxies, and that their spectral energy distribution (SED) was best replicated by a model where a clumpy shell of dust surrounds the starburst. Ferrara et al. (1999) calculated the effect of dust in various analytical disk plus bulge models, also using a Monte-Carlo model. Silva et al. (1998) and Charlot & Fall (2000) modeled dust effects using a simple two-phase model, where young stars are located in dense molecular clouds while older stars are extinguished only by the diffuse ISM, and showed that their models could fit spectral energy distributions of various observed galaxies. However, all these models had numerous free parameters and gave little guidance on how to choose them, thus limiting their predictive capability.

Notable previous efforts at simulating merging galaxies using hydrodynamic N-body codes with star formation and feedback are Mihos & Hernquist (1994, 1996) and Springel (2000), but these efforts did not consider realistic observations of their simulations including the effects of dust. Bekki & Shioya (2001, 2000a,b) did use a simple model for dust attenuation and reradiation along with N-body simulations to investigate major mergers. However, their modeling, using the “sticky particle” method

Electronic address: patrik@ucolick.org
Electronic address: tcx@cfp.harvard.edu
Electronic address: joel@scipp.ucsc.edu
Electronic address: somerville@stsci.edu

¹ Present address: Harvard-Smithsonian Center for Astrophysics, 60 Garden Street, Cambridge, MA 02138

(Schwarz 1981) and with no supernova feedback, did not allow them to capture essential features of the hydrodynamics of merging galaxies. This work builds on these earlier works, using a full radiative-transfer model to study the effects of dust in the most comprehensive and sophisticated suite of major-merger simulations done so far. The radiative-transfer model is described in Jonsson (2004)², and details about the hydrodynamic simulations can be found in Cox (2004)³ and Cox et al. (2005).

In this paper, we emphasize one particular aspect of these simulations: the presence of a tight correlation between the fraction of energy absorbed and quantities such as the luminosity, metallicity, and mass of the simulated systems. These relations should be useful for theoretical modeling of dust absorption in galaxies, for example in semi-analytic models of galaxy formation. This paper is the first in a series describing the effects of dust in the simulations, the appearance of the simulations and comparisons to observed starburst galaxies (Jonsson et al. and Lotz et al., in preparation) including using new nonparametric measures of morphology (Lotz et al. 2004). Other papers based on these simulations concern the creation of a halo of hot, shock-heated gas around the merger remnant (Cox et al. 2004), the star-formation properties of minor as well as major merger simulations (Cox et al., in preparation),

2. MODEL DESCRIPTION

The simulations, performed with the “entropy-conserving” version of the GADGET SPH code (Springel et al. 2001; Springel & Hernquist 2002), consist of encounters of identical copies of the galaxies listed in Table 1. Because of the very large parameter space, the number of simulations needed to exhaustively sample all possible initial conditions would be prohibitively large (on the order of thousands). Instead, the strategy used was to define a few reasonably realistic cases based on information from observations and cosmological simulations.

The main differences from previous work are the inclusion of efficient supernova feedback, a correct normalization of the star-formation law, and an accurate treatment of hydrodynamics (Cox et al. 2005). These served to make the merger-induced starbursts less intense. Peak star-formation rates for major mergers of typical late-type spiral galaxies are generally in the range $30 - 50 M_{\odot} \text{ yr}^{-1}$, except for very short spikes.

2.1. Model Galaxies

Several different dynamically self-consistent disk-galaxy models, listed in Table 1, are used in this study.

The Sbc galaxy was modeled using median properties for Sbc galaxies from Roberts & Haynes (1994) and bulge information from de Jong (1996). Lower- and higher-mass variants of the Sbc galaxy, called Sbc- and Sbc+, respectively, were modeled using the 25th and 75th percentiles of the distributions of properties. Another set of galaxies, the “G-series”, was based on mean relations from the Sloan Digital Sky Survey (Shen et al. 2003), gas properties from Bell et al. (2003), and bulge information from de Jong (1996). These galaxies have

² Available at <http://sunrise.familjenjonsson.org/thesis>.

³ Available at <http://physics.ucsc.edu/~tj/work/thesis>.

TABLE 1

THE GALAXY MODELS USED FOR THE MERGER SIMULATIONS.

Model	$M_{\text{vir}}^{\text{a}}$ (M_{\odot})	M_{b}^{b} (M_{\odot})	f_{g}^{c}	$V_{\text{rot}}^{\text{d}}$ (km s^{-1})	Z^{e} (Z_{\odot})
Sbc+	$9.28 \cdot 10^{11}$	$1.56 \cdot 10^{11}$	0.58	210	1.12
Sbc	$8.12 \cdot 10^{11}$	$1.03 \cdot 10^{11}$	0.58	195	1.00
G3	$1.16 \cdot 10^{12}$	$6.22 \cdot 10^{10}$	0.20	192	1.00
Sbc-	$3.60 \cdot 10^{11}$	$4.98 \cdot 10^{10}$	0.58	155	0.70
G2	$5.10 \cdot 10^{11}$	$1.98 \cdot 10^{10}$	0.24	139	0.56
G1	$2.00 \cdot 10^{11}$	$7.00 \cdot 10^9$	0.29	103	0.40
G0	$5.10 \cdot 10^{10}$	$1.60 \cdot 10^9$	0.38	67	0.28

NOTE. — For the Sbc galaxies, 9 mergers with different orbital geometries were used. For the other galaxies, only a prograde-prograde encounter was used.

¹ Virial mass.

² Baryonic mass.

³ Gas fraction (of baryonic mass).

⁴ Circular velocity.

⁵ Metallicity (gas and stellar).

significantly less gas than the Sbc models and cover a much larger range in mass. Detailed information about these and other model galaxies can be found in Cox (2004). The galaxies were assigned a metallicity consistent with Zaritsky et al. (1994), used for both the stellar SEDs and the initial gas metallicity. All in all, the seven galaxy models cover a range of about 100 in baryonic mass, 3 in gas fraction, and 4 in metallicity.

2.2. Galaxy Merger Setup

Identical pairs of each of the seven galaxies in Table 1 were put on a parabolic orbit with the disks prograde. One of the disks was in the plane of the orbit, while the other was tilted by 30° . Eight additional mergers of the Sbc galaxies were also simulated, exploring variations in galaxy orientation and encounter orbit. Details about the merger setup can be found in Cox (2004).

2.3. Radiative-Transfer Model

The Monte-Carlo radiative-transfer code *Sunrise*, similar to the DIRTY code (Gordon et al. 2001), is described in detail in Jonsson (2004) and in a future paper. Briefly, the geometry of gas and stars along with the detailed star-formation histories of the galaxies at roughly 50 different points in time were taken from the N-body simulations and used as inputs to the radiative-transfer calculation. Outputs are multi-wavelength images of the system from a number of viewpoints, as well as luminosity absorbed by dust and reradiated in the infrared. *Sunrise* is available to interested prospective users.⁴

The stellar SEDs were taken from the Starburst99 (v4.0, Leitherer et al. 1999) stellar population synthesis model. The IMF used, similar to a Kroupa IMF (Kroupa 2002), has a high-mass slope of -2.35 from the upper limit of $150 M_{\odot}$ down to $1 M_{\odot}$. Below this mass it is flat down to the lower limit of $0.1 M_{\odot}$. The disk stars existing at the start of the simulation were assumed to have been forming at a uniform rate for the previous 8 Gyr. The bulge stars were assumed to have formed in an instantaneous burst 8 Gyr earlier.

⁴ The Sunrise web site is <http://sunrise.familjenjonsson.org>.

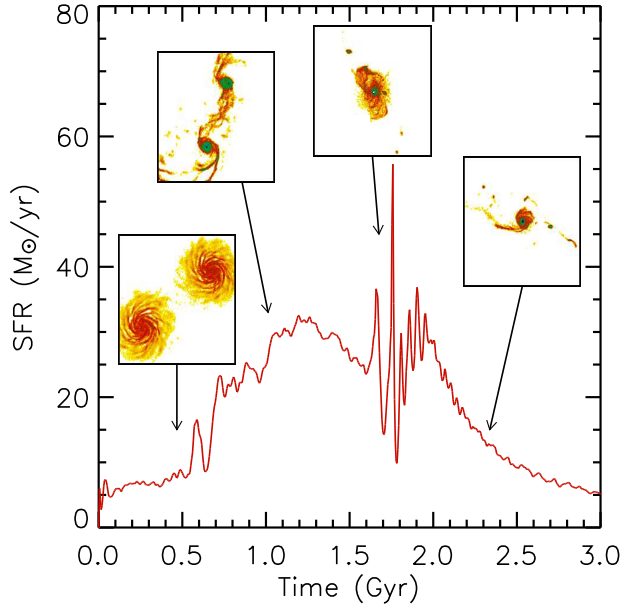


FIG. 1.— Overview of a major-merger event. The graph shows star-formation rate as a function of time for the prograde-prograde merger between two Sbc galaxies. The figures show the distribution of gas in the simulations at the indicated points in time from a viewpoint perpendicular to the orbital plane.

To be able to describe the simulation geometry with sufficient accuracy while keeping computational requirements reasonable, *Sunrise* uses an adaptive grid. The grid refinement criteria are adjustable; the parameters used are described in Jonsson (2004). The number of cells in the resulting grids ranged from around 70,000 at the start of the simulation to almost 300,000 at the time of peak star-formation rate and highest densities.

The dust grain model used was the “ $R = 3.1$ ” Milky-Way model by Weingartner & Draine (2001) with a dust-to-metal ratio $m_d/m_m = 0.4$ (Dwek 1998). The radiative-transfer calculation was performed for 22 different wavelengths between 21 nm and $5 \mu\text{m}$, including the $\text{H}\alpha$ and $\text{H}\beta$ nebular emission lines. One million Monte-Carlo rays were traced for each wavelength. Rather than self-consistently computing the infrared dust-emission spectrum, the templates of Devriendt et al. (1999), interpolated to the correct luminosity, were used.

3. RESULTS

First, some general results from the radiative-transfer simulations will be presented. Then we will continue with the specific results concerning dust attenuation in the simulations. Throughout this paper, “attenuation” will be understood to refer to the fraction by which luminosity is decreased due to dust, either averaged over all directions or along a specific line of sight. The term attenuation is preferred over absorption to emphasize that both absorption and scattering processes in a complex geometry contribute to a net decrease (or, in rare cases, increase) in the emerging radiation.

3.1. Overview of a Major Merger

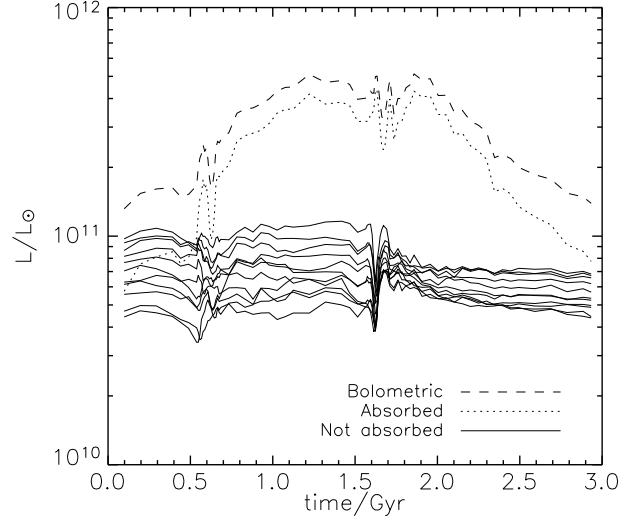


FIG. 2.— Time evolution of bolometric luminosity and dust attenuation for the prograde-prograde Sbc merger simulation. The bolometric luminosity of the system is shown with a dashed line, while the amount of luminosity absorbed by dust and reradiated in the infrared is shown with a dotted line. The solid lines show the luminosity *not* absorbed by dust, emerging in the UV/visual (more precisely the luminosity inferred by an observer under an assumption of isotropy), one line for each of the 11 viewing angles. The luminosity emerging in the UV/visual is practically independent of the bolometric luminosity and shows significant variation with viewing angle.

While the detailed behavior of a galaxy merger depends on the initial setup of the two galaxies, the general sequence of events remains the same. Figure 1 shows the star-formation rate of a merger between two Sbc galaxies, along with images of the system at different points in time. As the two galaxies initially approach each other, they are largely unaffected by each other’s presence. Tidal forces disrupt the galaxy disks at the time of the first close passage. The star-formation rate then increases due to gas being driven to the centers as the galaxies separate. The star-formation rate remains elevated as the galaxies turn around and again approach. There are several short bursts of star formation as the two components merge. After coalescence, the merger remnant relaxes, and the star-formation rate trails off over a timescale of about 1 Gyr.

The evolution of the bolometric luminosity of the same simulation is shown in Figure 2. The bolometric luminosity of the system increases by almost an order of magnitude during the course of the merger, closely following the star-formation rate, as expected for a star-burst system where young stars dominate the energy output. However, the fraction of luminosity which is absorbed by dust scales with luminosity in such a way that the luminosity *not* absorbed by dust typically stays almost constant. As the star-formation rate and hence the luminosity increase, the column densities of gas and dust also go up, and with them the attenuation; the two factors appear to conspire to keep the UV/visual luminosity roughly constant. This effect can be seen in Figure 2, where the solid lines, showing the luminosity escaping in different directions, show little vari-

ation with time. This tendency was also observed by Bekki & Shioya (2000a) in their simulations, and in observational studies (Adelberger & Steidel 2000).

While there is little temporal variation in the luminosity not absorbed by dust, there is, in general, a substantial difference between the flux escaping in different directions. Because the initial systems consist of disk galaxies, radiation escapes preferentially out of the plane of the galaxies. This creates a difference of around a factor of 2 in the escaping flux, clearly visible in Figure 2. The merger remnant is more spheroidal and thus the difference with viewing angle is smaller at the end stage of the mergers. As will be shown below, this variation in viewing angle means that quantities not dependent on direction, such as the fraction of bolometric luminosity which is absorbed, can be predicted with significantly smaller scatter than directional quantities like the emerging luminosity in a specific direction.

3.2. Simulated Images and Spectra

As mentioned in the model description, the outputs from the radiative-transfer calculations are multi-wavelength images from a number of viewpoints or, more precisely, an SED for each pixel in the images. To facilitate comparisons with observations, it has been integrated into images in a number of broadband filters (listed in Table 3) covering wavelengths from the GALEX FUV band to the IRAC2 band on the Spitzer Space Telescope and also collapsed into a spatially integrated SED. In total, about 25 major-merger simulations have been run through the radiative-transfer code, each at roughly 50 points in time. For each point in time, images and spectra have been generated from 11 viewpoints, equally distributed in solid angle, and in 12 different filters. This results in a grand total of roughly 10^5 images and 10^4 spectra. The analysis of these is the subject of a companion paper (Jonsson et al., in preparation), but to illustrate the outputs generated some images are shown in Figure 3 and a corresponding spectrum in Figure 4.⁵

3.3. Comparing to Observations

In order to determine how well our simulations mimic actual starburst galaxies, they must be compared to observations. While this comparison is described in Jonsson (2004) and is the subject of a companion paper, example results are included here to illustrate that the simulations appear to replicate the properties of observed galaxies. After accounting for dust effects, the simulations have an absolute r -band magnitude in the range -21.5 to -22.5 and a $u - r$ color of 1.3 to 2.2, falling in the region of bright, blue galaxies in the Sloan Digital Sky Survey (Baldry et al. 2004). Even 1 Gyr after the merger, there is enough ongoing star formation in the merger remnant that it is among the blue galaxies. In recent simulations, Springel et al. (2005a,b) have shown that feedback from an active galactic nucleus can help truncate star formation, which would let the merger remnant redden more quickly. In any case, the inclusion of dust is crucial for the agreement; without it, the systems are far too bright and blue to agree with observed galaxies.

⁵ Movies and the full set of color images of the merger simulations can be found on the Internet at <http://sunrise.familjenjonsson.org/thesis>.

The simulations were also compared to observations by Meurer et al. (1999, hereafter MHC) and Heckman et al. (1998). Both of these studies looked at correlations between dust attenuation and other properties of starburst galaxies. MHC looked at the relation between dust absorption, indicated by the far-infrared over ultraviolet flux ratio, and the ultraviolet spectral slope. In a sample of moderately luminous starburst galaxies observed by International Ultraviolet Explorer (IUE) and IRAS, they found a fairly tight correlation between the two parameters. However, Goldader et al. (2002) examined a small sample of more luminous LIRGs and ULIRGs, and found that they depart from the relation seen by MHC in the sense that their UV color is too blue for their infrared luminosity. When the same quantities are extracted from the simulations, the agreement, shown in Figure 5, is remarkable. The simulations follow the MHC relation when similar-luminosity systems are selected. In contrast, when the highest-luminosity subsample of the simulated galaxies is selected, they are found in the same region as the LIRGs/ULIRGs of Goldader et al. (2002). It should be emphasized that this is not a result of fitting the simulations to these observations, but rather a prediction of our initial conditions which were selected, a priori, to be realistic for local spiral galaxies. Unlike in earlier studies (Gordon et al. 1997), this agreement is contingent on the use of Milky-Way dust. SMC-type dust leads to far too red ultraviolet slopes and is inconsistent with the MHC relation in our simulations.

Heckman et al. (1998) studied correlations between dust absorption, infrared and ultraviolet luminosity, metallicity, absolute magnitude, etc. The agreement with those results, though not shown here, is also encouraging. These, while not exhaustive tests, indicate that our simulations provide a good replication of local starbursts. A future paper (Jonsson et al., in preparation) will explore the comparison between simulations and observations in detail.

The simulations can also be used to study the performance of star-formation indicators in the presence of dust. While the far-infrared luminosity provides a robust indication of the star-formation rate for starburst systems, both the $H\alpha$ and the ultraviolet luminosity suffer from severe dust effects (Jonsson 2004). Published dust corrections based on the Balmer line ratio (Calzetti et al. 1994) or the ultraviolet spectral slope (Bell & Kennicutt 2001) improve the estimate, but the star-formation rate can still be underestimated by up to an order of magnitude at the highest luminosities, where the dust corrections perform the worst. A detailed analysis of the star-formation indicators in the presence of dust is planned for a future paper.

3.4. Dust Attenuation

Looking at the nine Sbc simulations shown in Figure 6, there is a tight correlation between the bolometric luminosity of the system and the bolometric dust attenuation, averaged over all directions. For a given bolometric luminosity a uniquely determined fraction of luminosity is absorbed by the dust; it does not seem to matter if the system consists of two barely-interacting disks, a merger-driven starburst (on various orbits), or a post-starburst remnant. Simulations using galaxies of different mass or metallicity follow similar correlations offset to higher or

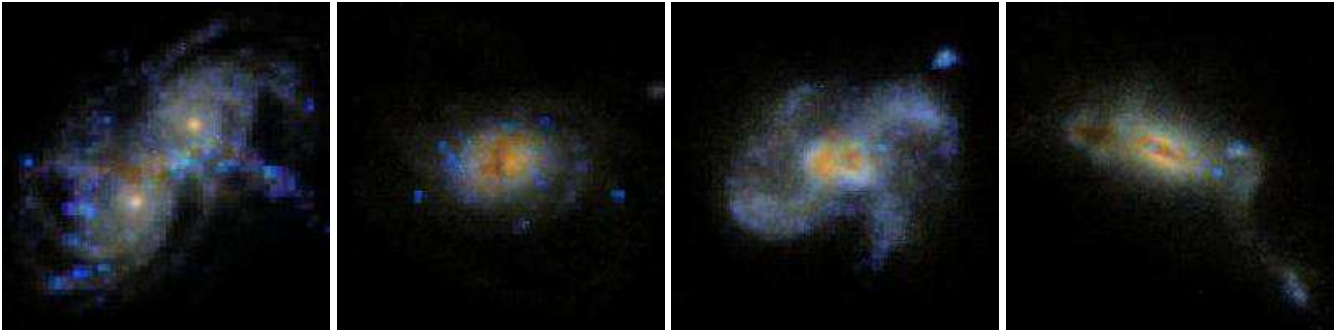


FIG. 3.— Images of the Sbc-Sbc prograde-prograde major merger at four different stages. On the left, about 0.6 Gyr into the simulation, the galaxies are passing each other for the first time. A line of induced star formation can be seen in the region between the two galaxies, where the gas in the two disks is being shocked. The next image, at 1.6 Gyr, shows the galaxies coming together for the second time. This collision is almost perfectly radial, concentrating a lot of gas and dust in the center, as evidenced by the clear dust lane. The third image, at 1.7 Gyr, shows the final coalescence of the two galaxies, with characteristic tidal tails. Finally, the rightmost image shows the merger remnant 2.0 Gyr after the start of the simulation. While the stellar distribution is largely spheroidal, a large fraction of the gas not consumed in the starburst has now cooled and reformed a disk, visible as a dust lane. (Disk reformation was also reported by Springel & Hernquist 2005.) The images cover 67 kpc squared and are in the SDSS g band. (The electronic edition shows urz color composite images generated using the algorithm of Lupton et al. 2003.)

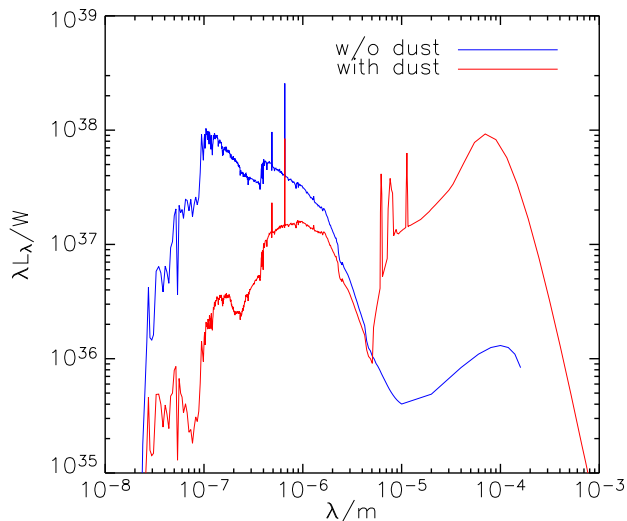


FIG. 4.— The spectral energy distribution associated with the second image of the Sbc-Sbc prograde-prograde major merger in Figure 3, 1.6 Gyr into the simulation. The solid (blue in the electronic edition) line shows the intrinsic stellar spectrum, while the dashed (red) line shows the emerging spectrum after taking dust attenuation into account. At wavelengths longer than $5\mu\text{m}$, the dust emission spectrum is taken from the templates of Devriendt et al. (1999). The two emission lines in the optical are $H\alpha$ and $H\beta$. In the ultraviolet, the dust attenuation is over an order of magnitude, and the signature of the well-known “2200Å bump” in the Milky-Way extinction curve is easily discernable.

lower attenuation.

Theoretically, it is expected that luminosity (for starbursting systems largely determined by star-formation rate) and dust absorption should correlate in the simulations, as both of these quantities are driven by gas density. Concentrating the gas to larger densities will increase the star-formation rate, and hence the bolometric luminosity, through the Schmidt law used. Concentrating the gas also increases the gas, and hence dust, column density, increasing dust absorption. Several observational studies have also concluded that dust attenuation generally seems to increase with galaxy

luminosity and star-formation rate (Wang & Heckman 1996; Adelberger & Steidel 2000; Hopkins et al. 2001; Sullivan et al. 2001; Vihj et al. 2003; Buat et al. 2004). In the following section, a toy model for estimating dust absorption will be presented. This will, in turn, motivate the fitting formula used to estimate the dust absorption in the simulations.

3.5. A Toy Model for Dust Attenuation

In order to come up with a simple model for how dust absorption should depend on luminosity, mass, and metallicity of a galaxy, consider a constant-density sphere of star-forming gas. For a sphere, the density is given by

$$\rho \propto M_g R^{-3}, \quad (1)$$

where M_g is the gas mass and R is the radius. According to the Schmidt law used to estimate the star-formation rate in the simulations, the star-formation rate density is

$$\dot{\rho}_* \propto \rho^{3/2}. \quad (2)$$

The total star-formation rate \dot{M}_* is thus

$$\dot{M}_* \propto M_g^{3/2} R^{-3/2}. \quad (3)$$

The optical depth of dust in the sphere will depend on the column density and the metallicity Z of the gas,

$$\tau \propto Z R \rho \propto Z M_g R^{-2}. \quad (4)$$

Eliminating R using equation 3, we get

$$\tau \propto Z \dot{M}_*^{4/3} M_g^{-1} \propto Z L^{4/3} M_g^{-1}, \quad (5)$$

where the last proportionality comes from assuming that the bolometric luminosity L is proportional to the star-formation rate. Finally, once the optical depth is determined, the absorbed fraction of luminosity (i.e., the attenuation) in a medium where luminous and absorbing material is uniformly mixed is given by (e.g. Calzetti et al. 1994)

$$\frac{L_{\text{abs}}}{L} = 1 - \frac{1}{\tau} (1 - e^{-\tau}). \quad (6)$$

Actually, equation 6 is appropriate for a plane-parallel slab, not a sphere. However, the purpose of the toy

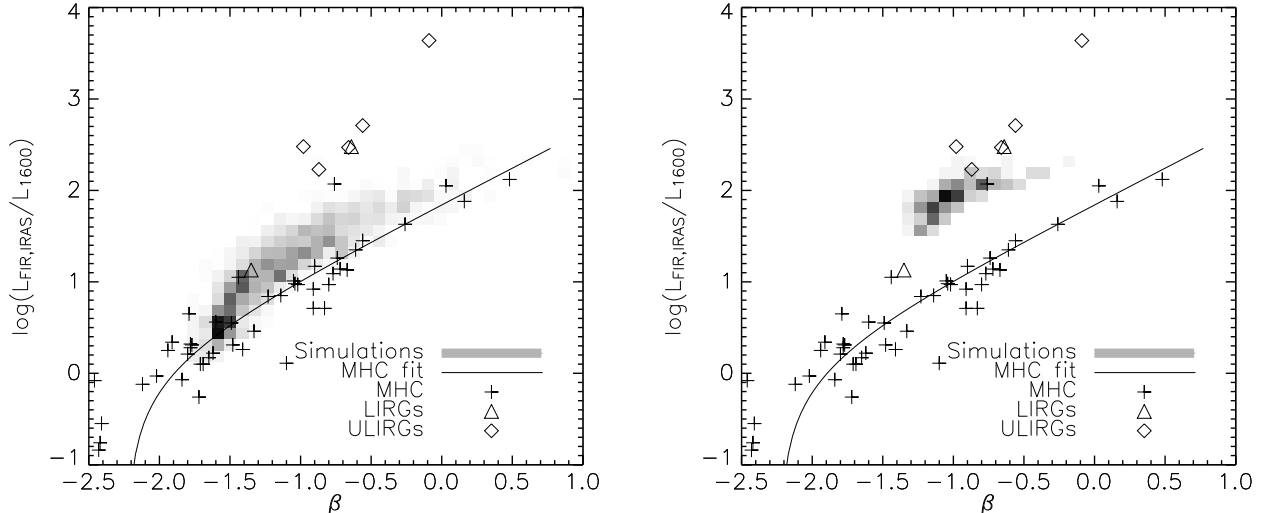


FIG. 5.— The relation between the IR/UV flux ratio and the UV spectral slope for the Sbc merger simulations (shaded region), compared to the results from Meurer et al. (1999, hereafter MHC, crosses) and Goldader et al. (2002, diamonds/triangles). On the left, only simulated galaxies with bolometric luminosity $L_{\text{bol}} < 2 \cdot 10^{11} L_{\odot}$ have been included. This low-luminosity sample agrees fairly well with the MHC correlation, which is for galaxies in this luminosity range. On the right, only the highest-luminosity simulated galaxies, with $L_{\text{bol}} > 7 \cdot 10^{11} L_{\odot}$ have been included. These points depart completely from the MHC galaxies and instead occupy the region of LIRGs/ULIRGs from the Goldader et al. (2002) sample. This agreement was not a result of fitting the models, but rather a prediction from our simulations, with no adjustment of parameters. This and other results indicate that our simulations provide a reasonably good replication of the properties of local starbursts.

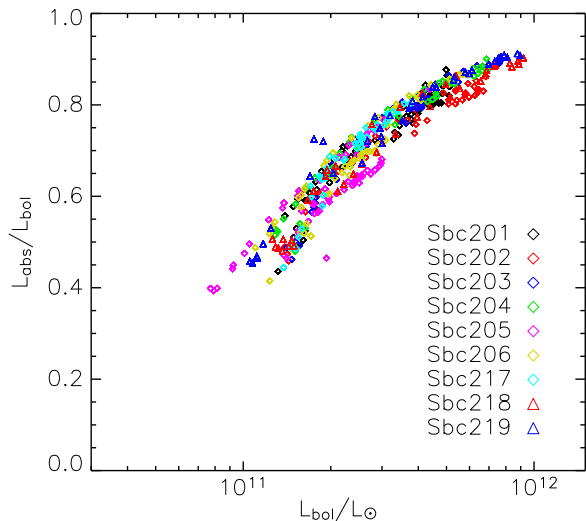


FIG. 6.— The relation between bolometric luminosity and attenuation (fraction of bolometric luminosity absorbed by dust, averaged over all directions) for the nine different Sbc-Sbc major merger simulations on various orbits. Each point is a simulation snapshot. For a given luminosity, the attenuations lie in a narrow range, regardless of encounter geometry, stage of merger and the fact that different simulations cover different luminosity intervals. All simulations were started with solar metallicity gas. (In the electronic edition, the different colors identify the different simulations in Appendix A of Cox 2004.)

model is to find a simple, physically motivated, fitting formula. As will be shown in the next section, equation 6 describes the behavior of the simulations well. Hence, in the interest of simplicity, it will be used.

This toy model has obvious limitations: It neglects scattering, and the exponents $4/3$ and -1 depend on the assumed geometry. Furthermore, the model is really more representative of an individual star-forming region than an entire galaxy, so included in the constant of proportionality in equation 5 is the number of such regions in the galaxy. If this number depends on the properties of the galaxy, a reasonable assumption, it will change the dependence on the different quantities in equation 5. Finally, the attenuation of the bolometric luminosity is an average of the attenuation at all wavelengths, and because the system in general is optically thick at short wavelengths and more or less optically thin at longer wavelengths, the behavior is more complicated than the simple equation 6. Real galaxies are thus more complicated than our assumptions, but our simple model gives a general description of the trends for the effects of dust.

3.6. Fitting Functions

While $L \propto \dot{M}_{\star}$ is a good approximation for starbursting galaxies, where young stellar populations dominate the luminosity, this assumption is not good in general. For this reason, simultaneous dependence on both L and \dot{M}_{\star} will be retained.

Guided by the toy model, one would expect the *gas* mass to be the dominant factor in the relation. However, fits using total *baryonic* (gas plus stars) mass, M_b , instead of gas mass had lower residuals. For this reason, baryonic mass is used for the fits.

Motivated by the above toy model and these considerations, the general fitting function to be used for the

TABLE 2
 FITS TO THE BOLOMETRIC ATTENUATION.

τ_0^a	α^a	β^a	γ^a	δ^a	σ^b	Comment
1.25	1.02	0.41	0.39	-0.82	0.04	Full fit
0.93	1.10		0.61	-0.68	0.04	Indep. of L
2.10	0.91	1.10		-1.03	0.05	Indep. of \dot{M}_*
2.09	0.94				0.14	Dep. on Z only.
2.34		0.28			0.12	Dep. on L only.
1.70			0.26		0.10	Dep. on \dot{M}_* only.
2.21				0.16	0.16	Dep. on M_b only.
0.32	0.30	-0.15	0.82	-0.52	0.05	Full fit with M_g^c

NOTE. — The attenuation is the fraction of bolometric luminosity which is absorbed, averaged over all directions.

¹ Parameter in equation 7.

² The standard deviation of the scatter around the fit.

³ This fit was performed with gas mass, instead of baryonic mass, driving the parameter δ in equation 7.

simulations is

$$\frac{L_{\text{abs}}}{L} = 1 - \frac{1}{\tau} (1 - e^{-\tau}), \text{ where}$$

$$\tau = \tau_0 \left(\frac{Z}{0.02}\right)^\alpha \left(\frac{L}{10^{11} L_\odot}\right)^\beta \left(\frac{\dot{M}_*}{M_\odot \text{ yr}^{-1}}\right)^\gamma \left(\frac{M_b}{10^{11} M_\odot}\right)^\delta, \quad (7)$$

and the Greek letters denote free parameters.

The fits were done as simple χ^2 minimizations, with one point for each simulation snapshot in the simulations listed in Table 1. As there were nine different Sbc merger simulations and only one of each of the simulations using the other galaxy models, the Sbc simulations were given only 1/9 the weight in the fits. This was done to avoid giving undue weight to the massive, bright, and gas-rich Sbc mergers. Because the time between saved simulation snapshots was varied in order to capture short-lived stages, each simulation snapshot was also weighted in proportion to its “time of influence”, i.e. the time to preceding and following snapshots. Apart from this weighting, constant errors on the points were assumed. Table 2 shows the parameters resulting from fits of the bolometric attenuation to the simulations under different constraints. The quantities come in with different powers from those in equation 6, but, as noted earlier, this is not surprising.

A plot of the actual attenuations against those predicted from the full fit is shown in Figure 7. The fit describes the behaviour of the simulations well, with a 1σ scatter of about 0.04 in the absorbed fraction. Since this fit describes the fraction of bolometric luminosity absorbed by dust, it can be used to predict the dust luminosity of these systems. It should be emphasized that the quantities used are those of the system, implying that when the merging galaxies are still distinct it is the aggregate luminosity, mass, and star-formation rate of the two which is used.

Table 2 contains additional parameter sets besides the complete fit. These are appropriate if some of the quantities which go into equation 7 are unknown. With a modest increase in the scatter around the relation, one of the largely complimentary quantities L or \dot{M}_* can be excluded. In these cases, the power of the quantity not excluded increases to assume the role of the excluded quantity. With significantly increased scatter, the attenuation can also be predicted from one quantity only. This is presumably because metallicity, luminosity, and

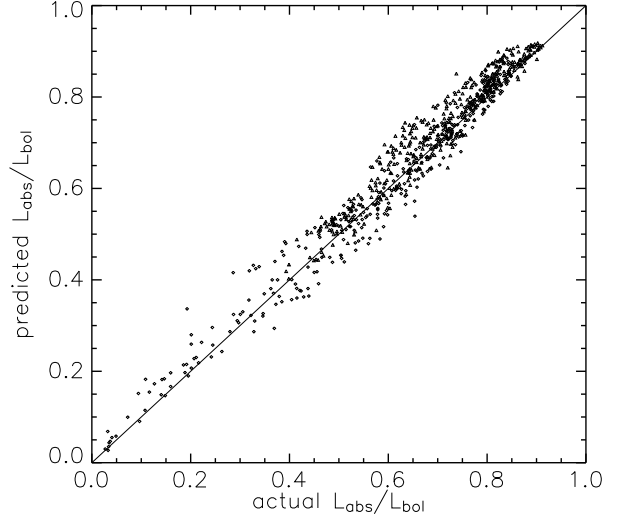


FIG. 7.— Actual attenuation (fraction of bolometric luminosity absorbed by dust) in the simulations, compared to the attenuation predicted by the full fit of equation 7 (the first line of Table 2). Each point is a simulation snapshot.

mass are intrinsically correlated in galaxies. It is difficult to say to what degree these single-parameter correlations are affected by our small set of galaxy models.

Finally, the last line of Table 2 contains the parameters obtained when the fit was done using the gas mass. The fit has about 50% larger scatter than when the baryonic mass was used, so it still provides a useful description of the data. However, the dependence on the quantities is strange, β is negative which means that more luminous galaxies should have *smaller* dust attenuation. It is as if luminosity has assumed part of the function of the baryonic mass.

3.7. Fits At Specific Wavelengths

The fits in the previous section are useful for predicting the infrared dust luminosity of the systems, but they cannot be used to predict the attenuation of radiation emerging from the system observed at a specific wavelength. Furthermore, in order to be able to make predictions of the luminosity inferred by an observer, the variation in attenuation with line of sight must be considered. Table 3 contains fits, also using equation 7, to the attenuation in each of the bandpasses included in the calculation. Here, each point in time of a simulation is associated with 11 different attenuations, one for each of the different viewing angles calculated. These fits have significantly larger scatter than the fit to the bolometric attenuation in Table 2, but this is largely due to the variation of attenuation over different lines of sight. When the attenuation is averaged over all lines of sight, the fit is unchanged, but the scatter is much smaller, only marginally larger than for the fit to bolometric attenuation. An example of a fit, for the SDSS g band, is shown in Figure 8.

3.8. Observations of Dust Attenuation

Several previous studies have attempted to estimate the dust attenuation in observed galaxies nature, and

TABLE 3
 FITS TO THE DUST ATTENUATION IN SPECIFIC FILTERS.

τ_0^a	α^a	β^a	γ^a	δ^a	σ^b	σ_i^c	Filter
7.67	3.33	-0.04	0.29	-0.74	0.07	0.04	GALEX FUV
5.03	2.45	0.03	0.36	-0.61	0.07	0.04	GALEX NUV
1.84	1.52	0.45	0.28	-0.70	0.10	0.05	SDSS <i>u</i>
1.27	1.39	0.55	0.19	-0.70	0.11	0.05	SDSS <i>g</i>
0.94	1.36	0.61	0.16	-0.71	0.12	0.05	SDSS <i>r</i>
0.78	1.34	0.65	0.12	-0.70	0.11	0.05	SDSS <i>i</i>
0.68	1.37	0.69	0.10	-0.72	0.11	0.05	SDSS <i>z</i>
0.53	1.43	0.72	0.09	-0.74	0.10	0.05	2MASS J
0.42	1.54	0.76	0.09	-0.78	0.09	0.05	2MASS H
0.32	1.62	0.77	0.10	-0.80	0.08	0.05	2MASS Ks
0.19	1.78	0.74	0.14	-0.82	0.06	0.04	Spitzer IRAC1
0.14	1.95	0.71	0.18	-0.86	0.06	0.04	Spitzer IRAC2
23.9		0.70			0.12	0.10	1900Å(WH96) ^d
4.0		0.49			0.15	0.11	B (WH96) ^d

NOTE. — Fits were performed using all parameters. The scatter in the far-ultraviolet bands is suppressed because most attenuations are close to 1.

¹ Parameter in equation 7.

² The standard deviation of the total scatter around the fit, including the variation with viewing angle.

³ The standard deviation of the intrinsic scatter around the fit, i.e. excluding the variation with viewing angle.

⁴ Fits done as a comparison to the study by Wang & Heckman (1996), described in section 3.8.

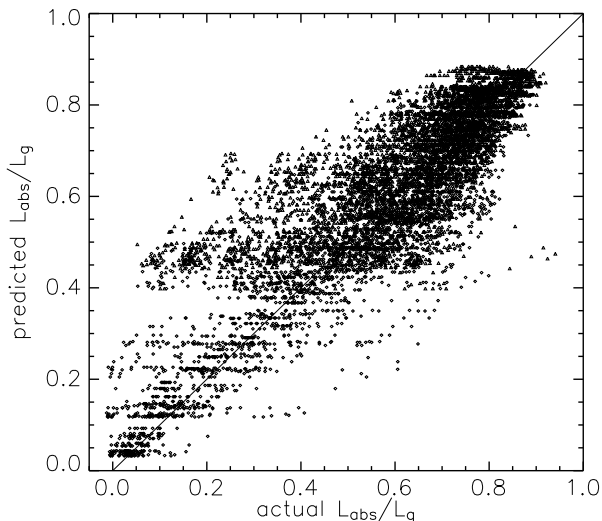


FIG. 8.— Actual attenuation in the simulations versus the attenuation predicted by equation 7, but now for the luminosity in the Sloan Digitized Sky Survey *g* band. Unlike Figure 7, which shows absorbed energy averaged over all lines of sight, this figure shows the line-of-sight attenuation. Each point is a simulation snapshot from a certain line of sight. The slightly negative attenuations result from preferential scattering out of the plane of the disk in the initial galaxies. This fit has significantly larger scatter than the fit to bolometric attenuation, a result mainly because of the large variation of attenuation with viewing angle, but provides a good description of the behavior averaged over all directions.

our simulations can be compared to these results.

Wang & Heckman (1996) examined the dust content in late-type galaxies based on their UV/FIR flux ratio and fit the derived optical depth to a power-law dependence on luminosity. To compare to their study, a fit of the ultraviolet attenuation using only a dependence on ultraviolet luminosity is also performed. This fit is

shown in Figure 9. This fit was complicated by the fact that when using only luminosity instead of all parameters to predict the dust attenuation, there is a significant difference between the initial merging galaxies and the merger remnants. Especially in the smaller G2, G1, and G0 mergers, the merger remnants have significantly higher dust attenuation for their luminosity compared to the earlier stages. Furthermore, because the simulated galaxies spend a lot of time as merger remnants (limited by how long the simulation has been run), this stage has significant weight when fitting. These points can be seen in the upper left of Figure 9. As discussed below, our model likely overestimates the dust attenuation in the merger remnants. For this reason, and also because WH96 did not include early-type galaxies, these low-luminosity, high-attenuation points were excluded in this fit. (If these points are included, the resulting fit, also shown in Figure 9, does not provide a good description for the low-luminosity pre-merger and merging galaxies.)

After excluding these points, the fit yields $\beta = 0.70$, consistent with the result of WH96 who obtained $\beta = 0.5 \pm 0.2$. In terms of the normalization, our fit results in $\tau_0 = 23.9$, at a luminosity of $10^{11} L_\odot$. Rescaled to the WH96 luminosity zeropoint of $4.5 \times 10^9 L_\odot$, it corresponds to a UV optical depth of 2.7, while their result was 1.7 ± 0.6 . The simulated galaxies seem to have larger optical depth for the same luminosity, possibly reflecting the fact that they not really “normal” spirals. However, the WH96 galaxies were essentially limited to $L_{1900} < 10^{10} L_\odot$, and in this luminosity range, the WH96 fit is a good description also of the simulated galaxies. The intrinsic scatter in this fit is much larger than when all the parameters are used.

WH96 also presented their results in terms of the B-band luminosity and, correspondingly, the attenuation in the B band. To compare to these result, a fit to the simulations was done in the B band (using the prescription of Fukugita et al. 1996 to transform the SDSS magnitudes into a B magnitude). The same points were excluded for this fit, also shown in Figure 9, as for the ultraviolet fit. This results in $\beta = 0.49$, in excellent agreement with WH96. Their normalization is lower also in this case. Our result was $\tau_0 = 4.0$, which, rescaled to the WH96 luminosity of $1.3 \times 10^{10} L_\odot$, corresponds to an optical depth of 1.5. Their result was 0.8 ± 0.3 .

A similar study was performed by Vijn et al. (2003), who estimated the UV attenuation in a sample of Lyman-break galaxies using radiative-transfer models of clumpy dust shells. They basically obtained

$$1 - \frac{L_{\text{abs}}}{L} \propto L^{-0.95 \pm 0.5}, \quad (8)$$

at 1600 Å. In optically thick situations, this would correspond to $\beta = 0.95 \pm 0.5$ in our formulation, also consistent with our result at 1900 Å.

Buat et al. (2004) compared the dust attenuation, in the GALEX NUV band, of two samples selected in the near-ultraviolet and far-infrared. While they saw an increase in dust attenuation with luminosity in both samples, they did not attempt to determine the luminosity dependence. No attempt has been made to replicate their selection criteria in our simulated galaxies either, but the distribution of attenuation with luminosity in the simu-

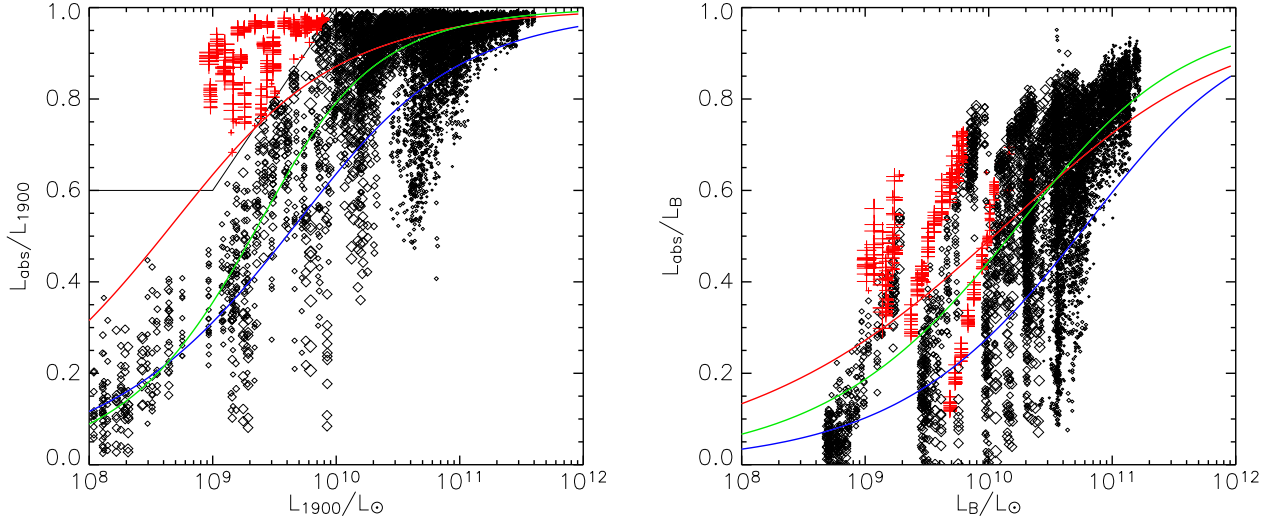


FIG. 9.— Comparison with Wang & Heckman (1996). On the left, luminosity at 1900 Å versus attenuation at 1900 Å for the simulations, on the right luminosity in the B band versus attenuation in the B band. The size of the symbols are proportional to the fitting weight of the points. The dashed (green in the Electronic Edition) lines show the fits marked “WH96” in Table 3. The points in the upper left region in the left plot, marked by the solid line, consist of merger remnants and were excluded from the fit for reasons explained in Section 3.7. Because these points are not nicely delineated in the right plot, they are also marked as (red) crosses. (The dotted (red) lines show the fits obtained if these points are included in the fit.) The dot-dashed (blue) lines show the WH96 fits. In the ultraviolet, the WH96 fit agrees fairly well with the simulated galaxies for luminosities $< 10^{10} L_{\odot}$, the maximum UV luminosity of the WH96 galaxies, but underpredicts the attenuation at high luminosities. In the B band, the WH96 fit has a luminosity dependence similar to our fit, but is normalized lower.

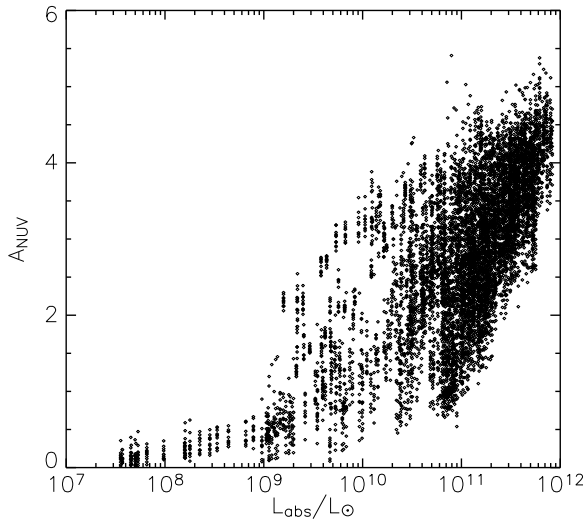


FIG. 10.— Luminosity absorbed by dust versus attenuation in the GALEX NUV band (in magnitudes) for the simulated galaxies. This plot can be directly compared to Figure 3 of Buat et al. (2004). Their infrared-selected galaxy sample shows a very similar distribution, while their UV-selected sample has lower attenuations. Given that our simulated galaxies are bright starbursts, the infrared selection is likely more appropriate, at least at higher luminosities. For $L_{\text{abs}} < 10^{10} L_{\odot}$, the Buat et al. (2004) IR-selected sample contains very few galaxies, probably a selection effect, but the ones present lie in the same region as the simulations.

lations (shown in Figure 10) is similar to that of their sample.

3.9. Model Limitations

While our suite of simulations is the most ambitious effort to self-consistently model dust extinction in starbursts so far, our model has limitations. For one, dust is known to be clumpy or patchy on small scales, something which is not taken into account in the simulations. Previous studies (Witt & Gordon 1996, 2000; Gordon et al. 1997) have indicated that clumping has important implications for the effects of dust. While the large-scale structure of the dust distribution in the galaxies is determined by the hydrodynamic simulations, clumping on the scale of individual star-forming regions is far below our resolution and is not included. The most likely effect of clumping would be to open up “holes” with lower attenuation, so that our simulations would underestimate the frequency with which young stellar populations are visible.

Another phenomenon which is treated poorly in our simulations is gas outflows. Starburst galaxies are almost ubiquitously observed to have large-scale gas outflows (e.g. Heckman et al. 2000). While our feedback prescription does provide energy input from supernovae, it does not seem to lead to significant outflows. Furthermore, recent simulations including active galactic nuclei (Springel et al. 2005b) show that AGN feedback can drive a powerful outflow, clearing out gas from the central regions of the galaxies. This phenomenon is also not included in our present simulations. In the context of dust attenuation, this lack of outflows has two implications. First, outflows, like dust patchiness, would tend to open up holes in the dust distribution. Second, the lack of outflows also means that the metals produced by the starburst remain in the starburst region. Since the optical depth is determined using a constant dust-to-metal ratio, this will translate to a larger opacity within the star-forming regions than would be expected if a signifi-

cant fraction of the metals were ejected.

Both of these limitations make it probable that our simulations overestimate the amount of dust attenuation to some degree, especially in the late stages after the galactic nuclei have merged. Less clear, however, is whether the correlations found here would be ruined. For example, while an AGN-driven outflow will clear out gas and dust from the galaxy and hence decrease the dust attenuation, it also truncates star formation. Thus, while the evolution of the (stellar) luminosity of the starburst would be altered by this phenomenon, the correlation between dust attenuation and the luminosity, metallicity, etc., of the starburst would not necessarily be altered. Work is underway to improve our model and include these effects.

4. DISCUSSION

One of the remarkable aspects of Figure 6 is that the low-luminosity stages of the simulations, which comprise both the initial, separate spiral galaxies and the final merger remnant, overlap. A priori, there seems to be no reason to expect that the attenuation should remain constant if two galaxies are merged into one. However, from the fit results in Table 2 it is evident that the powers of the extensive quantities L , \dot{M}_* , and M_b approximately add to zero. This results in a dust attenuation which is almost insensitive to simple size scaling of the galaxies; rather than being determined by luminosity or star-formation rate alone, the dust attenuation seems to be governed by “specific luminosity” and “specific star-formation rate”, i.e., L/M_b and \dot{M}_*/M_b . This is fortunate for our analysis, since it means that not treating the two galaxies in the initial stages of the merger separately does not bias the results. This is only true in the specific case being treated here, where the two galaxies are identical. If the two galaxies were not identical, as when simulating minor mergers or a merger between a spiral and an elliptical galaxy, the dust attenuation would have to be determined separately for the two components regardless of whether α , β , and γ sum to zero.

It should, however, be pointed out that $\alpha + \beta + \gamma \approx 0$ is a poor approximation for the fits to the attenuation in the GALEX bands in Table 3. There is thus the possibility that the fits in these bands have been biased by the use of system, rather than individual galaxy, quantities. Indeed, there is a significant discrepancy between the fits and the initial stages of the simulations in these bands, such that the fits overestimate the amount of dust attenuation.

Looking at the parameter sets in Table 3, clear trends with wavelength can be seen. Going from ultraviolet to near-infrared wavelengths, the dependence on star-formation rate decreases while the dependence on luminosity increases. This is not unexpected; the luminosity in the ultraviolet is dominated by massive, short-lived stars, and hence correlates well with star-formation rate. At longer wavelengths, contributions to the luminosity come from stars of a wide range in age and is better represented by the bolometric luminosity of the galaxy. This trend with wavelength thus contains information about the stars whose radiation is being absorbed. What is more surprising is that the trend is reversed at wavelengths longer than $2\ \mu\text{m}$. Naively, one would expect that the dust attenuation at progressively longer wave-

lengths always would be more dominated by older stars, but this does not seem to be the case. This effect probably originates in the fact that around the age of 10 Myr, a stellar population is very bright in the near-infrared due to the presence of red supergiants. This means that young stellar populations make a larger contribution to the emission at several μm than what is expected from their main-sequence temperatures.

It was earlier noted that, as shown in Figure 2, the UV/visual luminosity not absorbed by dust essentially is independent of the intrinsic bolometric luminosity. This notion is confirmed by the fit to the bolometric attenuation independent of the star-formation rate in Table 2. That fit yielded $\beta = 1.10$, close to $\beta = 1$ for which the increase in luminosity is exactly compensated by the increase in attenuation given by equation 6 (in the optically thick limit).

Is the fact that the dust attenuation in the simulations is well described by equation 7 indicating something about the relative geometry of dust and stars in the simulations? As already mentioned, gas density is the driving factor behind both dust optical depth and star-formation rate. Furthermore, in the simulations, dust and stars are assumed to be uniformly mixed within individual grid cells. It is thus not unreasonable to expect that a uniform mixture of dust and stars should fit the simulations reasonably well.

The fact that the dust attenuation can be predicted so well by a simple formula also implies that there are no hidden parameters determining whether a luminous galaxy will be a ULIRG or not. Bekki & Shioya (2000b), from analyzing a prograde-prograde and a retrograde-retrograde major merger at the time of highest star-formation rate, drew the conclusion that retrograde mergers should have stronger internal dust attenuation than prograde ones. This led them to conjecture that interacting galaxies without long tidal tails should be more prevalent among ULIRGs. This result is not confirmed by our much more extensive analysis. While there is a tendency for retrograde mergers to induce slightly more intense starbursts in our simulations, and hence be more obscured according to our fitting formula, they follow the same relation for dust attenuation as mergers of any other geometry. At least within the parameter space covered by these simulations, there should be no such thing as a “naked” vigorously star-forming, $10^{12} L_\odot$ system. While the attenuation along some lines of sight might be smaller, the vast majority of the bolometric luminosity should always be emerging as infrared dust emission.

Comparing the studies of Wang & Heckman (1996) and Vijn et al. (2003) to these simulation results, it is encouraging to note that the dependence of optical depth on luminosity is similar. Unfortunately, they did not have metallicity or mass information, so they were unable to perform a multi-dimensional fit like the one in this study. It would be interesting to know whether the dependence on these parameters would also be similar to what is found here.

The fitting formulae presented here are in the “theoretical plane”, i.e., they depend on quantities such as total baryonic mass and bolometric luminosity which are generally known in theoretical models but hard to determine from observations. As such, they are of limited use for interpreting observations. It has already been emphasized

that dust effects cancel the effects of increased luminosity to a remarkable degree, so that the simulations show virtually no correlation between the *apparent* luminosity and the dust attenuation, either bolometric or in the ultraviolet. Unfortunately, this implies that drawing conclusions about these highly dust-extinguished systems from their apparent luminosity is very difficult, unless infrared data are available. In particular, “correcting” apparent luminosities for dust using a luminosity-based prescription is not likely to work well, a fact also noted by Hopkins et al. (2001).

The relations presented here should be suitable for inclusion in theoretical models for galaxy formation, such as semi-analytic models (SAMs) including merger-driven starbursts (e.g., Somerville et al. 2001). Unlike other theoretical models for dust effects (e.g., Silva et al. 1998; Charlot & Fall 2000) our results give information about the *magnitude* of the dust attenuation and its dependence on the properties of the galaxy in a self-consistent way. Current approaches used to incorporate dust in SAMs include relying on empirical results like those of WH96 or even simpler approximations such as a uniform slab with optical depth proportional to gas column density times metallicity (essentially the toy model presented here). Even in more sophisticated models, such as those of Granato et al. (2000), the optical depth is typically determined in the same simple way. These models also contain numerous adjustable parameters whose values are not given by the SAM and thus must be fixed at constant values. Given that our fits appear to work well across a wide range of galaxy properties, including these results in SAMs should lead to a more realistic estimation of the effects of dust in cosmological scenarios.

Finally, nothing has been said here about the *shape* of the dust attenuation curve, e.g., if the simulated galaxies obey the “Calzetti law” (Calzetti et al. 1994). This information is contained in our fits, and a future paper will explore this in detail. For now, we simply remark that our simulations are inconsistent with a simple “screen-like” attenuation curve like the Calzetti law, and do not even follow any single reddening law resulting from more complicated geometries (Witt & Gordon 1996; Gordon et al. 1997). This is likely the result of a stochastic superposition of many star-forming regions with various optical

depths and ages.

5. SUMMARY

We have presented results from radiative-transfer calculations in a comprehensive suite of galaxy merger simulations. The results from these simulations consist of images at many different wavelengths, as well as spectral energy distributions, and seem to agree well with observed properties of starburst galaxies.

It was discovered that the dust attenuation (defined as the fraction of luminosity which is absorbed by dust) in the simulations can be predicted from the bolometric luminosity, star-formation rate, baryonic mass, and average gas metallicity of the system through a simple, physically motivated formula (eq. 7). Averaged over all directions, the attenuation of the bolometric luminosity can be predicted with a scatter of 4%. The attenuation along a specific line of sight can be predicted with a scatter of 6 – 12%, depending on wavelength. The increased scatter is largely a result of the variation of attenuation with viewing angle. These relations are valid for simulations with a range of two orders of magnitude in mass, with metallicities from 0.3 to $1.1 Z_{\odot}$, and gas fractions from 20 to 60%. The relations also seem to be valid for both isolated and interacting galaxies.

Our results are consistent with studies of observed galaxies by Wang & Heckman (1996) and Vijn et al. (2003), but our inclusion of additional independent variables significantly lowers the scatter around the relations, and we present results valid for wavelengths from the far-ultraviolet to the near-infrared.

We thank Volker Springel for making GADGET and his initial-conditions generator available to us. We also thank Jennifer Lotz and Kathy Cooksey for useful feedback on a draft version of this paper. This research used computational resources of the National Energy Research Scientific Computing Center (NERSC), which is supported by the Office of Science of the U.S. Department of Energy and also UpsAnd, a Beowulf at UCSC. PJ was supported by a grant from IGPP/LLNL, TJC and JRP by grants from NASA and NSF.

REFERENCES

- Adelberger, K. L., & Steidel, C. C. 2000, ApJ, 544, 218
 Baldry, I. K., Glazebrook, K., Brinkmann, J., Ivezić, Ž., Lupton, R. H., Nichol, R. C., & Szalay, A. S. 2004, ApJ, 600, 681
 Bekki, K., & Shioya, Y. 2000a, ApJ, 542, 201
 —. 2000b, A&A, 362, 97
 —. 2001, ApJS, 134, 241
 Bell, E. F., & Kennicutt, R. C. 2001, ApJ, 548, 681
 Bell, E. F., McIntosh, D. H., Katz, N., & Weinberg, M. D. 2003, ApJ, 585, L117
 Buat, V. et al. 2004, ApJS, in press (astro-ph/0411343)
 Calzetti, D., Kinney, A. L., & Storchi-Bergmann, T. 1994, ApJ, 429, 582
 Charlot, S., & Fall, S. M. 2000, ApJ, 539, 718
 Cox, T. J. 2004, PhD thesis, UC Santa Cruz
 Cox, T. J., Jonsson, P., Primack, J., & Somerville, R. S. 2005, MNRAS, submitted
 Cox, T. J., Primack, J., Jonsson, P., & Somerville, R. S. 2004, ApJ, 607, L87
 de Jong, R. S. 1996, A&A, 313, 45
 Devriendt, J. E. G., Guiderdoni, B., & Sadat, R. 1999, A&A, 350, 381
 Dwek, E. 1998, ApJ, 501, 643
 Elbaz, D., & Cesarsky, C. J. 2003, Science, 300, 270
 Ferrara, A., Bianchi, S., Cimatti, A., & Giovanardi, C. 1999, ApJS, 123, 437
 Fukugita, M., Ichikawa, T., Gunn, J. E., Doi, M., Shimasaku, K., & Schneider, D. P. 1996, AJ, 111, 1748
 Goldader, J. D., Meurer, G., Heckman, T. M., Seibert, M., Sanders, D. B., Calzetti, D., & Steidel, C. C. 2002, ApJ, 568, 651
 Gordon, K. D., Calzetti, D., & Witt, A. N. 1997, ApJ, 487, 625
 Gordon, K. D., Misselt, K. A., Witt, A. N., & Clayton, G. C. 2001, ApJ, 551, 269
 Granato, G. L., Lacey, C. G., Silva, L., Bressan, A., Baugh, C. M., Cole, S., & Frenk, C. S. 2000, ApJ, 542, 710
 Heckman, T. M., Lehnert, M. D., Strickland, D. K., & Armus, L. 2000, ApJS, 129, 493
 Heckman, T. M., Robert, C., Leitherer, C., Garnett, D. R., & van der Rydt, F. 1998, ApJ, 503, 646
 Hopkins, A. M., Connolly, A. J., Haarsma, D. B., & Cram, L. E. 2001, AJ, 122, 288
 Jonsson, P. 2004, PhD thesis, UC Santa Cruz

- Kroupa, P. 2002, in ASP Conf. Ser., ed. E. K. Grebel & W. Brandner, Vol. 285 (San Francisco: ASP), 86–
- Leitherer, C. et al. 1999, ApJS, 123, 3
- Lotz, J. M., Primack, J., & Madau, P. 2004, AJ, 128, 163
- Lupton, R., Blanton, M. R., Fekete, G., Hogg, D. W., O’Mullane, W., Szalay, A., & Wherry, N. 2003, astro-ph/0312483
- Meurer, G. R., Heckman, T. M., & Calzetti, D. 1999, ApJ, 521, 64
- Mihos, J. C., & Hernquist, L. 1994, ApJ, 431, L9
- . 1996, ApJ, 464, 641
- Roberts, M. S., & Haynes, M. P. 1994, ARA&A, 32, 115
- Sanders, D. B., & Mirabel, I. F. 1996, ARA&A, 34, 749
- Schwarz, M. P. 1981, ApJ, 247, 77
- Shen, S., Mo, H. J., White, S. D. M., Blanton, M. R., Kauffmann, G., Voges, W., Brinkmann, J., & Csabai, I. 2003, MNRAS, 343, 978
- Silva, L., Granato, G. L., Bressan, A., & Danese, L. 1998, ApJ, 509, 103
- Smail, I., Ivison, R. J., & Blain, A. W. 1997, ApJ, 490, L5
- Somerville, R. S., Primack, J. R., & Faber, S. M. 2001, MNRAS, 320, 504
- Springel, V. 2000, MNRAS, 312, 859
- Springel, V., Di Matteo, T., & Hernquist, L. 2005a, ApJL, in press (astro-ph/0409436)
- . 2005b, MNRAS, submitted (astro-ph/0411108)
- Springel, V., & Hernquist, L. 2002, MNRAS, 333, 649
- . 2005, ApJL, submitted (astro-ph/0411379)
- Springel, V., Yoshida, N., & White, S. D. M. 2001, New Astronomy, 6, 79
- Sullivan, M., Mobasher, B., Chan, B., Cram, L., Ellis, R., Treyer, M., & Hopkins, A. 2001, ApJ, 558, 72
- Vijh, U. P., Witt, A. N., & Gordon, K. D. 2003, ApJ, 587, 533
- Wang, B., & Heckman, T. M. 1996, ApJ, 457, 645
- Weingartner, J. C., & Draine, B. T. 2001, ApJ, 548, 296
- Witt, A. N., & Gordon, K. D. 1996, ApJ, 463, 681
- . 2000, ApJ, 528, 799
- Wolf, C. et al. 2004, ApJ, submitted (astro-ph/0408289)
- Zaritsky, D., Kennicutt, R. C., & Huchra, J. P. 1994, ApJ, 420, 87